# 3 Dimensional numerical model of holographic grating formation in photopolymer materials

Haoyu Li, Yue Qi, Ra'ed Malallah, and John T. Sheridan[*]

School of Electrical, Electronic and Communications Engineering, UCD Communications and Optoelectronic Research Centre, SFI-Strategic Research Cluster in Solar Energy Conversion, College of Engineering and Architecture, University College Dublin, Belfield, Dublin 4, Ireland.

## ABSTRACT

When the large thickness is used as the holographic storage materials, a non-ignorable problem is the light intensity attenuation in depth due to high absorptive of the dye. For this reason more completely modeling the evolutions inside the material is necessary to consider into the developed standard kinetic model. In this paper the photo-polymerization processes during the large thickness holographic grating formation are analyzed. A 3-dimensional algorithm is present by deriving the system partial differential rate equations governing each associated chemical species, and using the finite difference approximation, these equations can be solved numerically. This extended model describes the time varying behaviors of the non-uniform photo-physical and the photochemical evolutions in photopolymer materials. In this model both dye molecules consumption and light energy absorption are calculated time varyingly, and then the polymer and monomer concentrations distributions are obtained. Applying the Lorenz-Lorenz relationship, the non-uniform grating formatted in material depth, and its refractive index, which is distorted from ideal sinusoidal spatial distribution, can be more accurately predicted.

Keywords: Holographic grating; Photopolymers; 3-dimensional kinetic model

## 1. INTRODUCTION

Photopolymers have been actively studied due to their high performances as holographic data storage material in recent years[1–5]. To optimize potential holographic memory capacity, preparing more large thickness gratings, governing more narrow width of Bragg angular selectivity curve, is an effective realistic way[6–8]. In order to further developments, a detailed understanding of what happened in physical depth during the photo-polymerization processes, has been ever more crucial[9–11]. Nevertheless, the recording illumination intensity has the attenuation inside as a result of high absorption of the dye in the large thickness of the gratings, generating the non-uniform and non-linear behaviors of the photo-physical and photochemical processes[12,13]. In any attempt to evaluate real storage capacity of such volume grating, a more complete 3-dimensional kinetic model is necessary.

Previously, extensive work has been presented discussing both the large thickness gratings and the photochemical mechanisms of the photopolymer materials. As Gallego et al.[14–16] described that there is a numerical attenuation coefficient of the light which is obtained by fitting the experimental results inside the material, which leads to an attenuation refractive index modulation inside the material, and the resulting effective optical thickness is smaller than its physical thickness. Gleeson et al.[17–21] had the detailed researches of the photo-absorptive behavior of the dye and photochemical evolutions during the grating formation, and the 1-dimensional nonlocal photo-polymerization driven diffusion (NPDD) model has been developed including the polymer chain growth and diffusion effects both during and post-exposure.

Based on these previous studies, in this paper, such a theoretical 3-dimensional model incorporating the photo-physical and photochemical effects in order to more accurately characterizing the non-uniform photo-polymerization processes is developed. In this model the spatial and temporal varying of the absorbed light intensity can be evaluated by Beer-Lambert law, and the non-uniform absorption is obviously when the dye is high sensitive. Depending on the non-uniform recording light energy absorption in depth, each component's concentration in 3-dimensional spatial distribution is estimated respectively, and then how the grating formation and the induced refractive index variation in depth are shown using the Lorentz-Lorentz relation[22–26]. Using the extended model, the non-uniform volume grating formation evolution involved in the material can be represented in 3-dimensionally.

This paper is structured as follows.  In Section 2, we briefly review the primary photochemical mechanisms involved the photo-initiation mechanisms and the photo-polymerizationl reaction occurring during the holographic grating formation.  The aim is to estimate the spatial light distribution inside the material and the photosensitizer absorptive behavior, and then the expression of the time varying attenuation of light intensity in depth is observed.  In Section 3, the extended 3-dimensional kinetic model including these above effects is derived.  Using the set of partial differential rate equations, the concentration distribution of each component involved is described.  These partial differential equations are simplified and solved numerically using the finite difference method.  Based on the Lorenz-Lorenz relationship the refractive index of the grating is derived.  In Section 4, the numerical simulation results are presented and discussed with detail.  Finally, a brief conclusion is provided in Section 5.

## 2.  PHOTOCHEMICAL MECHANISM

The work carried out in this section contains two major parts.  The first subsection provides the material photo-initiation mechanisms aiming to analyze the time varying photosensitizer absorption behavior and calculate the light intensity attenuation in depth.  Subsection 2.2 briefly describes the photo-physical and photochemical evolutions in the photo-polymerization systems and present how the volume grating formatting by estimating the refractive index variation.

### 2.1  Photo-initiation mechanisms

During the suitable illumination of a layer the photosensitizer absorbs a photon, and the ground state dye molecule, Dye, is promoted to a singlet excited state, $^1$Dye* [27–30],

$$Dye + h\nu \xrightarrow{k_{aS}} {}^1Dye^*, \tag{1}$$

where $k_{aS}$ (s$^{-1}$) is the rate of photon absorption in the ground state.  The excited singlet state can recover to its ground state, and the resulting singlet state dye molecule can also undergo intersystem crossing into triplet state $^3$Dye*, as Gleeson described [19].  We combine the generative process of the triplet state dye,

$$Dye + h\nu \xrightarrow{k_{aT}} {}^3Dye^*, \tag{2}$$

where $k_{aT}$ (s$^{-1}$) is the rate from the ground state to triplet state which can also return to the ground state as pervious study shown[27–30].  The singlet state dye molecules recover processes as,

$$^1 ye^* \xrightarrow{k_r} Dye, \tag{3}$$

where $k_r$ (s$^{-1}$) is constant the rate of recovery of the excited state dye back to ground state; Dye is represented ground state dye; and the $^1$Dye* is represented the excited singlet state dye.  As previously described, the primary radicals $(R^{\bullet})$[17–21] is produced when the triplet state dye reacts with the co-initiator (electron donor, ED).  The major reactions taking place are as follows:

$$^3 ye^* + ED \xrightarrow{k_d} R^{\bullet} + HDye^{\bullet}, \tag{4}$$

$$ED + HDye^{\bullet} \xrightarrow{k_b} H_2 \; ye + ED_{int}, \tag{5}$$
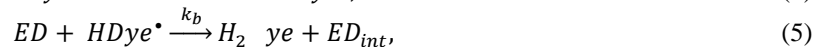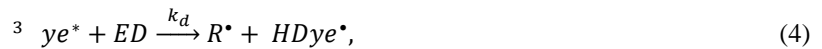
where $^3$Dye* represents the triplet state dye; $HDye^{\bullet}$ represents a radicalized dye; $H_2Dye$ is the di-hydro transparent form of the dye; and $ED_{int}$ is an intermediate form of the co-initiator.  $k_d$ (cm$^2$ mol$^{-1}$ s$^{-1}$ ) is the rate constant of dissociation of the initiator and $k_b$ (cm$^2$ mol$^{-1}$ s$^{-1}$ ) is the rate constant of bleaching.  All of these photoreactions are summarized in Figure 1.
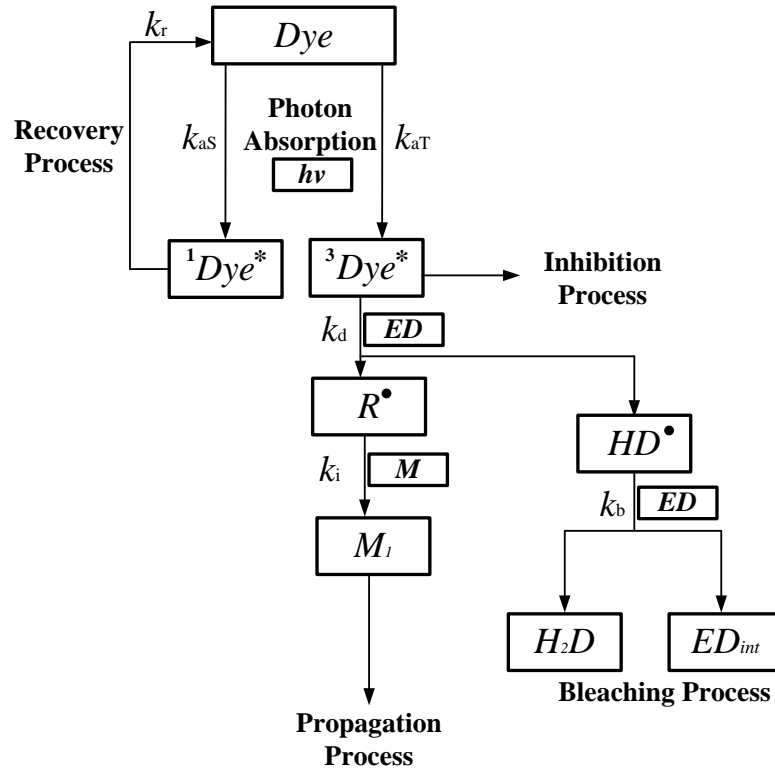
Figure 1. Flow chart illustrating the photo-initiation mechanisms.

Based on the Beer-Lambert law and the generations in photo-initiation[27–30], we assume the time varying light intensity in depth (z-axis), $I_{in}{}'$ (z,t) (Einstein $cm^{-3}$ $s^{-1}$), during the dye excitation can be written:

$$I_{in}{}'(z,t) = T_{sf}(z)I_0{}'\{exp[-\varepsilon_D \int_0^z [Dye(z',t)]dz']\}/z, \qquad (6)$$

where $I_0{}'$ (Einstein $cm^{-2}$ $s^{-1}$) is the incident intensity, $\varepsilon_D$ ($cm^2$ $mol^{-1}$) is the molar absorption coefficient of the photosensitizer, and $[Dye(z',t)]$ (mol $cm^{-3}$) is the time vary ground state dye concentration distribution in depth which is involved in a variable upper limit integral function, $\int_0^z [Dye(z',t)]dz'$. $T_{sf}(z) = T_s(z) \times T_f(z)$ is a fraction associated the energy lost by Fresnel and scattering which are varying with the layer's depth [27–30]. Applying the finite difference method [14–16], the Eq. (6) can be calculated numerically. If we take a small step $\Delta z$ along z-axis, then the value of the light intensity can be considered being a small numerical error [31]. Using this approximation, both the concentration of each component and incident intensity can be regarded as closing to uniform distribution in the 'small step' $\Delta z$ of the material film in depth. In this way we divide the total thickness of the material film $d$ (cm) into different sub-films and its thickness is written as $d_l$ (cm). The sum of the thickness can be given

$$d = \sum_{l=1}^{L} d_l, \qquad (7)$$

where $L$ is the number of divided sub-films chosen. Thus the variable $z$ can be written as $z = id_l$ where i is an integer and $1 \leq i \leq L$. To do so Eq. (6) can be simplified into 1-dimensional equation to calculate the intensity in sub-film as follows

$$^iI_{in}{}'(t) = {}^iT_{sf}I_0{}'\{exp[-\varepsilon_D d_l \sum_{j=0}^{i-1}[{}^jDye(t)]]\}/(id_l), \qquad (8)$$

where $^iI_{in}{}'$ (t) (Einstein $cm^{-3}$ $s^{-1}$) is the time varying incident intensity in the ith sub-film; $^iT_{sf}$ is the Fresnel and scattering losses in the depth from the surface to the ith sub-film; and $\sum_{j=0}^{i-1}[{}^jDye(t)]$ (mol $cm^{-3}$) denotes the sum of the time vary ground state dye concentration from the sub-film which is near the surface to the $i$th sub-film. We define that when $i = 1$, the dye concentration $[^0Dye(t)]$ regards the air closing to the first sub-film material layer and defining $[^0Dye(t)] = 0$. As denoted in Eq. (6) it is clear that when the light is propagating to the $i$th sub-film there has an attenuation due to the absorption by the photosensitizer and Fresnel and scattering losses from first sub-film to the ($i$th − 1) sub-film. It is also necessary to convert the photo-detector measures mW $cm^{-2}$ into Einstein $cm^{-3}$ $s^{-1}$, and this can be done using[19, 20, 28]

$$I_0{}' = [\frac{I_0 \lambda B}{N_m hc}], \qquad (9)$$

where $I_0$ (mW cm$^{-2}$) is the incident intensity; $\lambda$ (nm) is the wavelength of incident beam; $N_m = 6.02 \times 10^{23}$ is the Avogadro's number; c (m s$^{-1}$) is the speed of light; h (J s) is Plank's constant. $B = 1 - \exp[-\varepsilon_D A_0 d_l]$ [19, 20] is the absorptive fraction in each sub-film which determines a material layer's initial absorptive capacity where $A_0$ (mol cm$^{-3}$) is the dye's initial concentration. To do so the time varying absorbed intensity $I_a(z, t)$ (Einstein cm$^{-2}$ s$^{-1}$) in depth can be presented:

$$I_a(z,t) = {}^i I_a(t) = [{}^{i+1}I_{in}'(t) - {}^i I_{in}'(t)]d_l,\tag{10}$$

where ${}^i I_a(t)$ (Einstein cm$^{-2}$ s$^{-1}$) denotes the light energy absorbed in $i$th sub-film.

## 2.2 Kinetic model

In the free radical photo-polymerization processes the kinetic model is based on the follows four main photochemical reactions processes [9–11, 17–21].

*Process I. Initiation.*

$$I \xrightarrow{h\nu} 2R^\bullet,\tag{11a}$$

$$R^\bullet + M \xrightarrow{k_i} M_1^\bullet.\tag{11b}$$

*Process II. Propagation.*

$$M_n^\bullet + M \xrightarrow{k_p} M_{n+1}.\tag{12}$$

*Process III. Termination.*

$$M_n^\bullet + M_m^\bullet \xrightarrow{k_{tc}} M_{n+m},\tag{13a}$$

$$M_n^\bullet + M_m^\bullet \xrightarrow{k_{td}} M_m + M_n,\tag{13b}$$

$$M_n^\bullet + R^\bullet \xrightarrow{k_{tp}} M_n R.\tag{13c}$$

*Process IV. Inhibition.*

$$R^\bullet + Z \xrightarrow{k_{Z,R^\bullet}} RZ^\bullet,\tag{14a}$$

$$M^\bullet + Z \xrightarrow{k_{Z,M^\bullet}} M_n Z^\bullet,\tag{14b}$$

$$^3\text{Dye}^* + Z \xrightarrow{k_{Z,D}} \textit{Leuco Dye}.\tag{14c}$$
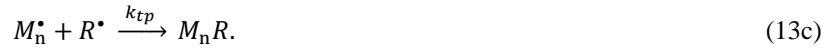
In the above set of chemical equations, $I$ is the iniator; $h\nu$ indicates the energy absorbed from a photon; $k_i$ is the chain initiation kinetic constant. $M$ represents a monomer molecule and $M_1^\bullet$ is the chain initiator; $k_p$ is the rate constant of propagation; $k_{tc}$ and $k_{td}$ are the rate constants of combination and disproportionation; $k_{tp}$ is the rate constant of primary radical termination; and $k_{Z,R}^\bullet$, $k_{Z,M}^\bullet$ and $k_{Z,D}$ are the rate constants of inhibition of the primary radicals, the macro radicals, and triplet state dye. Z is the inhibitor; $M_n$, $M_m$, $M_{m+n}$, $M_n R$, $RZ^\bullet$ and $M_n Z^\bullet$ represent polymer species and dead polymers. In some of the previous work[17–20, 27–30], the rate of generation of primary radical and the polymerization rate of the radical chain polymerization system, $R_i$ (mol cm$^{-3}$ s$^{-1}$) and $R_p$ (mol cm$^{-3}$ s$^{-1}$), can be derived by,

$$R_i = 2\Phi I_a(z,t),\tag{15}$$

$$R_p = k_p[M^\bullet(x,z,t)][u(x,z,t)].\tag{16}$$

where $\Phi$ is the number of primary radicals initiated per photon absorbed and the absorbed intensity $I_a(z,t)$ can be obtained by Eq. (10). $[M^\bullet(x,z,t)]$ (mol cm$^{-3}$) represents the macro-radicals concentration and $[u(x,z,t)]$ (mol cm$^{-3}$) is the concentration of the free monomer, which can be derived in Section 3.

# 3. MODEL DEVLOPMENT

Based on flow diagram and chemical equations presented[9–11, 17, 20], we derive following set of partial differential equations representing the evolutions of the material concentrations.

$$\frac{\partial[\text{Dye}(x,z,t)]}{\partial t} = -k_{aS}(x,z,t)[\text{Dye}(x,z,t)] - k_{aT}(x,z,t)[\text{Dye}(x,z,t)] + k_r[\text{SDye}^*(x,z,t)],\tag{17}$$

$$\frac{\partial[\text{SDye}^*(x,z,t)]}{\partial t} = k_{aS}(x,z,t)[\text{Dye}(x,z,t)] - k_r[\text{SDye}^*(x,z,t)],\tag{18}$$

$$\frac{\partial[\text{TDye}^*(x,z,t)]}{\partial t} = k_{aT}(x,z,t)[\text{Dye}(x,z,t)] - k_d[\text{TDye}^*(x,z,t)][ED(x,z,t)] - k_{z,D}[\text{TDye}^*(x,z,t)][Z(x,z,t)],\tag{19}$$

$$\frac{\partial [ED(x,z,t)]}{\partial t} = -k_b[\text{HDye}^\bullet(x,z,t)][ED(x,z,t)] - k_d[\text{TDye}^*(x,z,t)][ED(x,z,t)],$$

(20)

$$\frac{\partial [\text{HDye}^\bullet(x,z,t)]}{\partial t} = k_d[\text{TDye}^*(x,z,t)][ED(x,z,t)] - k_b[\text{HDye}^\bullet(x,z,t)][ED(x,z,t)],$$

(21)

$$\frac{\partial [R^\bullet(x,z,t)]}{\partial t} = k_d[\text{TDye}^*(x,z,t)][ED(x,z,t)] - k_i[R^\bullet(x,z,t)][u(x,z,t)] - k_{tp}[R^\bullet(x,z,t)][M^\bullet(x,z,t)]$$
$$- k_{z,R^\bullet}[R^\bullet(x,z,t)][Z(x,z,t)],$$

(22)

$$\frac{\partial [M^\bullet(x,z,t)]}{\partial t} = k_i[R^\bullet(x,z,t)][u(x,z,t)] - k_t[M^\bullet(x,z,t)]^2 - k_{tp}[R^\bullet(x,z,t)][M^\bullet(x,z,t)]$$
$$- k_{z,M^\bullet}[R^\bullet(x,z,t)][Z(x,z,t)],$$

(23)

$$\frac{\partial [u(x,z,t)]}{\partial t} = \frac{\partial}{\partial x}\left\{D_m(x,t)\frac{\partial [u(x,z,t)]}{\partial x}\right\} + \frac{\partial}{\partial z}\left\{D_m(z,t)\frac{\partial [u(x,z,t)]}{\partial z}\right\} - k_i[R^\bullet(x,z,t)][u(x,z,t)]$$
$$- \int_0^d \int_{-\infty}^\infty k_p[M^\bullet(x',z',t)][u(x',z',t)]G(x,x',z,z')\,dx'dz',$$

(24)

$$\frac{\partial [N(x,z,t)]}{\partial t} = -\frac{\partial}{\partial x}\left\{D_N(x,t)\frac{\partial [N(x,z,t)]}{\partial x}\right\} - \frac{\partial}{\partial z}\left\{D_N(z,t)\frac{\partial [N(x,z,t)]}{\partial z}\right\}$$
$$+ \int_0^d \int_{-\infty}^\infty k_p[M^\bullet(x',z',t)][u(x',z',t)]G(x,x',z,z')\,dx'dz',$$

(25)

$$\frac{\partial [Z(x,z,t)]}{\partial t} = \frac{\partial}{\partial x}\left\{D_Z(x,t)\frac{\partial [Z(x,z,t)]}{\partial x}\right\} + \frac{\partial}{\partial z}\left\{D_Z(z,t)\frac{\partial [Z(x,z,t)]}{\partial z}\right\} - k_{z,D}[\text{TDye}^*(x,z,t)][Z(x,z,t)]$$
$$- k_{z,R^\bullet}[R^\bullet(x,z,t)][Z(x,z,t)] - k_{z,M^\bullet}[M^\bullet(x,z,t)][Z(x,z,t)] + \tau_Z\{Z_0 - [Z(x,z,t)]\}.$$

(26)

In these equations $[\text{Dye}(x,z,t)]$ (mol cm$^{-3}$) represents the ground state dye concentration; $[\text{SDye}^*(x,z,t)]$ (mol cm$^{-3}$) represents the singlet state excited dye concentration; $[\text{TDye}^*(x,z,t)]$ (mol cm$^{-3}$) represents the triplet state excited dye concentration; $[ED(x,z,t)]$ (mol cm$^{-3}$) is the co-initiator's (electron donor) concentration; $[\text{HDye}^\bullet(x,z,t)]$ (mol cm$^{-3}$) represents the radicalized dye concentration; $[R^\bullet(x,z,t)]$ (mol cm$^{-3}$) represents the primary radicals concentration; $[N(x,z,t)]$ (mol cm$^{-3}$) is the polymer concentration; and $[Z(x,z,t)]$ (mol cm$^{-3}$) is the inhibitor's concentration. $D_m(x,t)$ (mol cm$^{-3}$) and $D_m(z,t)$ (mol cm$^{-3}$) represent the monomer diffusion rate along the $x$ and $z$ axis direction; $D_N(x,t)$ (mol cm$^{-3}$) and $D_N(z,t)$ (mol cm$^{-3}$) represent the polymer diffusion rate along the $x$ and $z$ axis direction; $D_Z(x,t)$ (mol cm$^{-3}$) and $D_Z(z,t)$ (mol cm$^{-3}$) represent the inhibitor diffusion rate along the $x$ and $z$ axis direction. $\tau_z$ is the rate of replenishing of oxygen (inhibitor) into the material layer from the surrounding environment.

$G(x,x',z,z')$ [17, 20, 32, 33] is the non-local material spatial response function along the $x$ and $z$ axis direction and given by

$$G(x,x',z,z') = \frac{1}{2\pi\sqrt{\sigma_x\sigma_z(1-\rho^2)}}\exp\frac{\left[-\frac{(x-x')^2}{2\sigma_x} - \frac{(z-z')^2}{2\sigma_z} + \frac{\rho(x-x')(z-z')}{\sqrt{\sigma_x\sigma_z}}\right]}{1-\rho^2};$$

(27)

where $\sigma_x$ and $\sigma_z$ are respectively the constant nonlocal response parameters normalized with respect to the grating period and the thickness, and $\rho$ is the correlation coefficient, and in this paper we assume the nonlocal response in $x$-axis and $z$-axis is independence so that $\rho = 0$. Domain of integration along $x$-axis in Eq. (27) demonstrate effect of initiation at location $x'$ and polymerized at location $x$ and the initial material distributing for $-\infty < x < \infty$. As to the $z$-axis in Eq. (27) describes the effect of initiation at location $z'$ and polymerized at location $z'$ and the initial material distributing for $0 < z < d$. In this model, $k_{aS}(x,z,t)$ (s$^{-1}$) and $k_{aS}(x,z,t)$ (s$^{-1}$) denote the photon absorptive rate varying from the ground state to the singlet state and triplet state. As Liu and Gleeson described [19, 20, 34] such photon absorptive rate can be written

$$k_{aS}(x,z,t) = \phi_S \varepsilon_D I(x,z,t)z,$$

(28a)

$$k_{aT}(x,z,t) = \phi_T \varepsilon_D I(x,z,t)z,$$

(28b)

where $\phi_S$ and $\phi_T$ (mol Einstein$^{-1}$) denote the quantum efficiencies of the reaction from ground state to the singlet and triplet state; and $I(x,z,t)$ (Einstein cm$^{-2}$ s$^{-1}$) is the incident intensity. We assume illumination by a sinusoidal exposure along the $x$-axis and the two exposing coherent beams the resulting interference pattern for symmetrically exposure is a periodic modulating distribution. Moreover the exposing area intensity and illuminated profile on the material surface is an ellipse for the recording beams at an incidence angle $\theta$. From the above the exposure 3-dimensional distribution in the material can be written:

$$I(x,z,t) = I_{in}'(z,t)[1 + V\cos(Kx)]\cos\theta,$$

(29)

where $K = 2\pi/\Lambda$ is the grating vector magnitude; $\Lambda$ is the formatted grating period; and $I_{in}'(z,t)$ (Einstein cm$^{-3}$ s$^{-1}$) is given using Eq. (6) in Section 2. The visibility of the fringes is given by $V = 2(I_1 I_2)^{1/2}/(I_1 + I_2)$, where $I_1$ and $I_2$ are the intensities of the two incident beams. Based on previous derivation in Section 2, the variable along $z$-axis can be approximately treated using the finite difference method and the variable along $x$-axis Eqs. (17)–(26) can also be written as Fourier series [17, 20]

$$X(x,z,t) = {}^{idl}X(x,t) = \sum_{j=0}^{\infty} {}^{idl}X_j(t)\cos(jKx),$$

(30)

where $X(x,z,t)$ represents the component in the photopolymer material; ${}^{idl}X(x,t)$ represents the 2-dimensional concentration $X(x,t)$ distributing in the $i$th sub-film and the variable $z$ equivalents to $z = i \times d_l$; and ${}^{idl}X_j(t)$ represents the time varying the $j$th harmonic Fourier series coefficients which is a 1-domensional function. Thus the partial differential rate equations with three dimensional variables are derived into the simple total differential rate equations and can be solved as Gleeson et al.did [17, 19, 20, 34].

During the formation of a volume holographic grating, the photo-polymerization processes are taking place spatially and temporally varying. From above derivation it is clear that along $z$-axis the grating formation is non-uniform. Using the Lorentz-Lorentz relation [22–24] the refractive index is obtained, and all material swelling and shrinkage effects are neglected.

$$\frac{[n(x,z,t)]^2 - 1}{[n(x,z,t)]^2 + 2} = \varphi^{(m)}(x,z,t)\left(\frac{n_m^2 - 1}{n_m^2 + 2} - \frac{n_b^2 - 1}{n_b^2 + 2}\right) + \varphi^{(p)}(x,z,t)\left(\frac{n_p^2 - 1}{n_p^2 + 2} - \frac{n_b^2 - 1}{n_b^2 + 2}\right) + \frac{n_b^2 - 1}{n_b^2 + 2},$$

(31)

where $n_m = 1.4719$, $n_p = 1.520$ and $n_b = 1.4957$ are the refractive indices of the monomer, polymer and background material. $\varphi^{(m)}(x, z, t)$ and $\varphi^{(p)}(x, z, t)$ are the respective volume fractions of monomer and polymer, which can be calculated by $\varphi_i = x_i v_i / \sum_i x_i v_i$, where $x_i$ is the molar fraction and $v_i$ is the molar volume of the $i$th component[17]. According to Eq. (31) the time varying refractive index can be obtained

$$n(x,z,t) = [(1 + 2\chi)/(1 - \chi)]^{1/2},$$

(32)

where $\chi = \varphi^{(m)}(x,z,t)\left(\frac{n_m^2 - 1}{n_m^2 + 2} - \frac{n_b^2 - 1}{n_b^2 + 2}\right) + \varphi^{(p)}(x,z,t)\left(\frac{n_p^2 - 1}{n_p^2 + 2} - \frac{n_b^2 - 1}{n_b^2 + 2}\right) + \frac{n_b^2 - 1}{n_b^2 + 2}$, and these volume fractions can be obtained by the material components' concentrations [17–21].

## 4. SIMULATION RESULTS AND DISCUSSION

We now wish to demonstrate that our developed model describing the 3-domensional varying behavior of the photopolymer materials; the holographic grating formation in depth; and investigating the variations of components' concentrations.

The spatial frequency chosen for the simulation is 1428 lines/mm. The exposing fringe visibility is unity, $V = 1$. The material layer thickness is $d = 300$ $\mu$m and the sub-film is $d_l = 10$ $\mu$m (the number of slices is $L = 30$). Two recording beams of wavelength, $\lambda = 532$ nm, delivering a total $(I_1 + I_2)$ exposing intensity of 10 mW cm$^{-2}$. The initial concentrations of the components of the photopolymer materials were chosen as follows. Dye, $[A_0] = 1.22 \times 10^{-6}$ (mol cm$^{-3}$); monomer, $[U_0] = 2.83 \times 10^{-3}$ (mol cm$^{-3}$); electron donor, $[ED_0] = 3.18 \times 10^{-3}$ (mol cm$^{-3}$); and inhibitor, $[Z_0] = 1 \times$

$10^{-8}$ (mol cm$^{-3}$). The $x$-axis rate parameters value used are $\sqrt{\sigma_x}$ = 50 nm, and the nonlocal effective along $z$-axis can be neglected because with the method of thickness division, the thickness of the resulting sub-film is very small comparing to the total material thickness. The diffusion coefficients along $x$-axis of oxygen and monomer are simplified, i.e., $D_Z(x,t) = D_Z$ and $D_m(x,t) = D_m$, where $D_m$, $D_Z$ and are the diffusion constants for monomer and inhibitor respectively, and they are taken to be constant, i.e., $D_z = 1.0 \times 10^{-8}$ cm$^2$ s$^{-1}$, $D_m = 1.0 \times 10^{-11}$ cm$^2$ s$^{-1}$. Similarly the diffusions along $z$-axis are not considered in our simulations. Other physical parameters for numerical predictions include $\varepsilon_D = 1.72 \times 10^8$ cm$^2$ mol$^{-1}$, $\phi_S = 6.0 \times 10^{-3}$ mol Einstein$^{-1}$, $\phi_T = 20.0 \times 10^{-3}$ mol Einstein$^{-1}$, $k_i = k_p = 1 \times 10^7$ cm$^3$ mol$^{-1}$ s, $k_{tp} = 10k_t = 1.0 \times 10^8$ cm$^3$ mol$^{-1}$ s$^{-1}$, $k_{z,R\bullet} = k_{z,M\bullet} = 3 \times 10^{12}$ cm$^3$ mol$^{-1}$ s$^{-1}$, $k_{z,D} = 1.1 \times 10^8$ cm$^3$ mol$^{-1}$ s$^{-1}$, $k_d = 4.3 \times 10^3$ cm$^3$ mol$^{-1}$ s$^{-1}$, $k_r = 0.33 \times 10^{-3}$ s$^{-1}$, and $k_b = 0.23 \times 10^2$ cm$^3$ mol$^{-1}$ s$^{-1}$. The Fresnel and scattering loss fraction $T_{sf}(z = 300 \ \mu m)$ is 0.75. These values generated the simulations in this section were estimated from fits to standard AA/PVA experimental data [18, 21, 34].
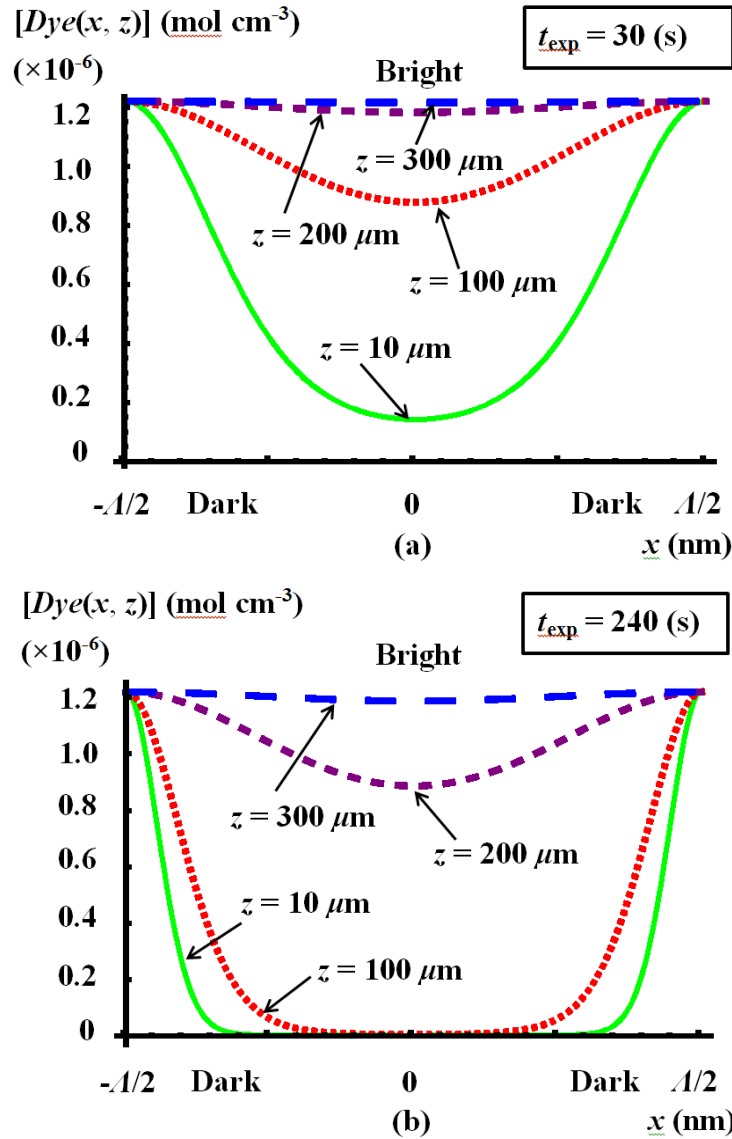


Figure 2. (color online) Simulations of the ground state dye distributing in $x$-$z$ axis [$Dye(x, z)$] mol cm$^{-3}$ for two different exposure times: case (a) $t_{exp}$ = 30 s and case (b) $t_{exp}$ = 240 s, for four different material depths: $z = 10 \ \mu m$ (green full curve); $z = 100 \ \mu m$ (red short dashed curve); $z = 200 \ \mu m$ (purple dashed curve); and $z = 300 \ \mu m$ (blue long dashed curve).

Substituting Eq. (8) into Eq. (28), and the set of partial differential equations can be solved numerically. Combining the spatial concentrations from all the harmonic amplitudes, the spatial distributions of the ground state dye, $[Dye(x,z)]$, can be observed form Figure 2. The results for four material depths: $z = 10~\mu m$; $z = 100~\mu m$; $z = 200~\mu m$; and $z = 300~\mu m$, are shown between the grating period $-\Lambda/2 \leq x \leq +\Lambda/2$. In order to provide a meaningful comparison, we choose two different exposure times to plot, case (a) $t_{exp} = 30$ s and case (b) $t_{exp} = 240$ s.

As can be observed in Figure 2, the ground state dye concentration is consumed due to the absorption of photons [27–30] in the bright region. In case (a) it can be noted that, in bright region the consumption of ground state dye molecules presents the apparent attenuating trend in material depth. This is due to the initial layer absorbance mainly depends on the illumination intensity because there are enough dye molecules in the early stage exposure. Based on the previous analysis, if the local position along $z$-axis is more close to the layer's surface, and it will has the higher intensity exposure, which leads to a more rapid consumption of the ground state dye than the deeper position. Then, as closing to the layer surface the exposure time increasing, in bright region the ground state dye molecules, are used up more rapidly, and more ground state dye molecules will be consumed in the dark region, which had been described by Shui et al.[37,38]. When $t_{exp} = 240$ s in case (b) the spatial distribution of ground state dye concentrations for different depths are distorting from the exposing sinusoidal pattern exhibiting narrowing in the dark region. A comparison can be carried out between $z = 10~\mu m$ and $z = 100~\mu m$. As the material depth is more close to the surface, the distortion is visibly stronger due to the higher intensity exposing. It is clear that there is a nonlinear response of the material to the exposure intensity, and in large thickness gratings such nonlinear response mainly performs as the variation of the material depth, because there is intensity attenuation along the material depth. Similarly both the spatial distributions of the primary radical concentration and the induced polymer concentration represent the deviations from the ideal sinusoidal distribution, which would be produced by given nonlinear response of the dye absorption. In summary, the polymer chain initiation is not directly proportional to the exposing interference patterns along $x$-axis. Then we can predict that the induced refractive index inside the material is not a simple monotone decreasing function for the depth position along $z$-axis as the exposing interference intensity varying at that point, which will be discussed in detail following.



(a)
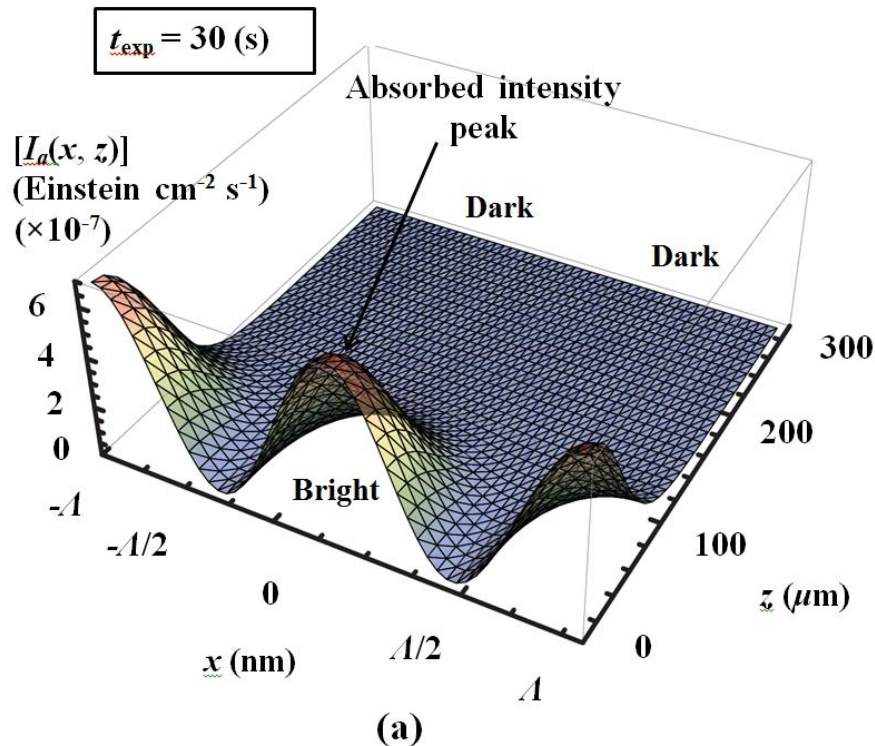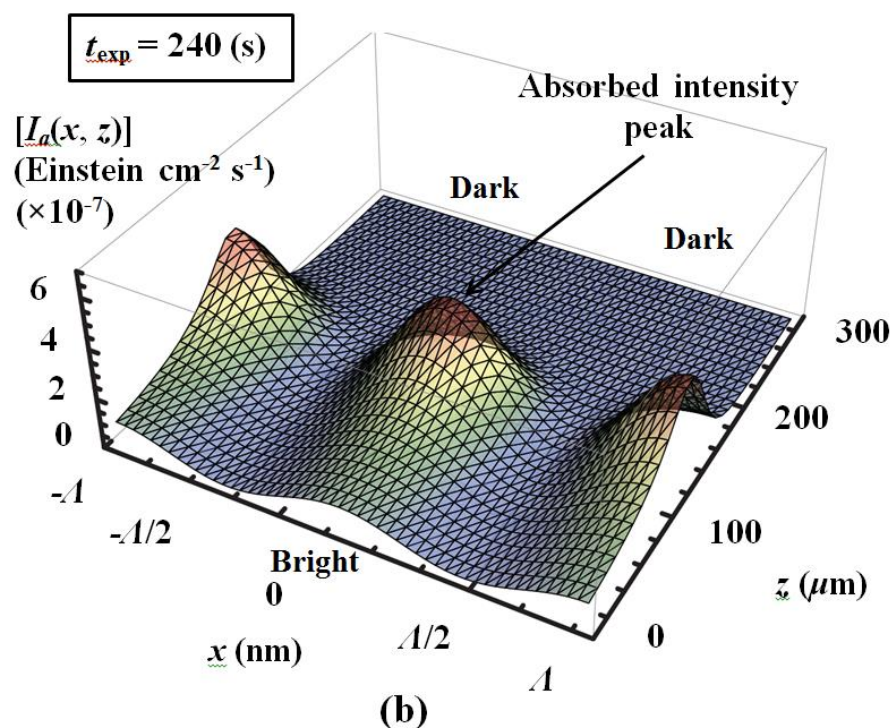
Figure 3. Comparison of absorbed intensity $I_a(x,z)$ Einstein cm$^{-2}$ s$^{-1}$ in depth, of the spatial frequency $SF$ = 1428 lines mm$^{-1}$ and incident intensity $I_0$ = 10 mW cm$^{-2}$, for different exposure times: case (a) $t_{exp}$ = 30 s and case (b) $t_{exp}$ = 240 s.

Such nonlinear material response can also be examined in a 3-dimensioanl view of time varying light absorption using Eq. (10). In Figure 3, $I_a(x,z)$ is plotted for two different exposure times, case (a) $t_{exp}$ = 30 s and case (b) $t_{exp}$ = 240 s. At the beginning of exposure time, such as case (a) in Figure 3, for the thinner position of the layer a higher percentage of the total absorptive dye concentration is used up much more rapidly. Corresponding to spatial and temporal variation of ground state dye concentration, the amplitude of $I_a(x,z)$ starts to increase as the ground state dye molecules are being excited more and more in bright region. When the dye consumption rate is most rapid, $I_a(x,z)$ will have a peak value. As shown in Figure 3 the absorbed intensity peak is turning up around the thinner location of the material. As the exposure continuing, for thinner position the relatively fewer absorptive dye molecules are available comparing to the thicker position. Meanwhile the effect of the light absorption begins to decrease in this certain area, and the transmitted light intensity will increase leading to another absorbed intensity peak in the thicker position of the layer. From pervious calculation model predictions, it is clear that when the highest percentage absorbed dye molecules being excited reaching to the $i$th sub-film, such available dye concentrations are both smaller in ($i$th − 1) and ($i$th + 1) sub-film. It means that the light intensity from the ($i$th − 1) sub-film is very high, nevertheless the light intensity comes from $i$th to ($i$th + 1) sub-film is small. For this reason the maximum dye consuming rate is moving along the material depth and the corresponding absorbed intensity peak will move from the position $z$ = 0 $\mu$m to the position $z$ = 300 $\mu$m as the exposing continuing. Furthermore, it should be specially noted that the peak value of photon absorption presents a slight attenuation as shown in Figure 3. This is because, when the light is propagating through the material, even though there is a highest absorptive dye concentration at a certain time point, but there is still some light energy can transmit to the deeper material. Thus during the whole exposure time the ground state dye concentration is always being consumed in material depth. When the absorbed intensity peak is reaching to the thicker position the available initial ground state dye concentration at this point is smaller than thinner position.
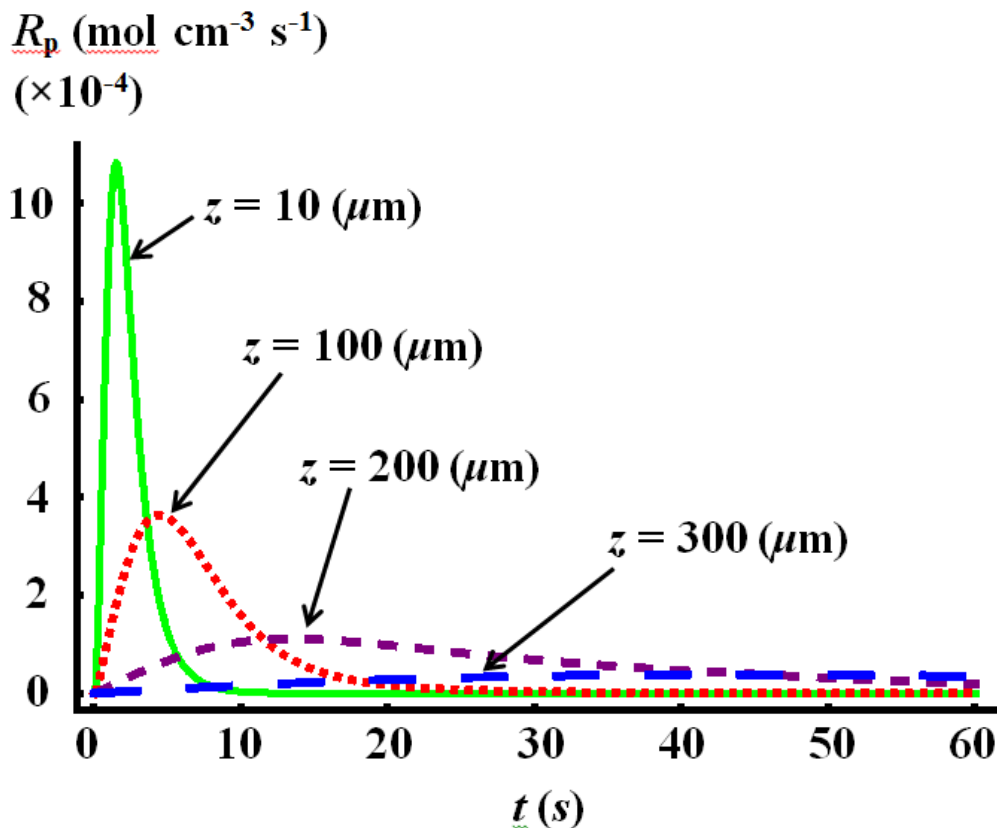
Figure 4. (color online) Simulation of the variation of polymerization rate, $R_p$ mol cm$^{-3}$ s$^{-1}$, during exposure for four different material depths: $z = 10$ $\mu$m (green full curve); $z = 100$ $\mu$m (red short dashed curve); $z = 200$ $\mu$m (purple dashed curve); and $z = 300$ $\mu$m (blue long dashed curve).

   Using the same simulation conditions and the 3-dimensional calculation model described above, by numerically solving for the concentrations $[M^{\bullet}(x,z,t)]$ (mol cm$^{-3}$) and $[u(x,z,t)]$ (mol cm$^{-3}$) respectively, the evolution of the polymerization rate, $R_p = [M^{\bullet}(x,z,t)][u(x,z,t)]$, can be examined. As can be seen from Figure 4, the time varying $R_p$, which appears in Eq. (16), is simulated for four different material depths: $z = 10$ $\mu$m; $z = 100$ $\mu$m; $z = 200$ $\mu$m; and $z = 300$ $\mu$m, summing the concentration amplitudes of all their harmonics. As the material depth is closing to the layer surface, the polymerization rate increases more rapidly arriving at a higher maximum value, and then it decreases more rapidly. This is because when focusing on the depth is 10 $\mu$m, and there will be the higher intensity as mentioned previously, and a great number of the photons available are absorbed, which leads to produce more radicals. A larger generally polymerization rate causes a more rapid conversion form monomers to polymers. Throughout the conversion polymerization rate will decrease quickly after reaching its maximum value. This because in the expression of the polymerization rate, $R_p = [M^{\bullet}][u]$, the macro-radicals concentration, $[M^{\bullet}]$, is decreasing quickly, due to there are less available dye molecules being excited after previous consuming and the termination of the growing polymer chains also leads to the reduction of $R_p$[20, 37, 38]. These results are presented in Figure 4, for the thicker position cases, the maximum value of $R_p$ is smaller and such time varying trends are slower duo to the lower light energy obtained from the exposure time $t_{exp} = 0$ to $t_{exp} = 60$ s.
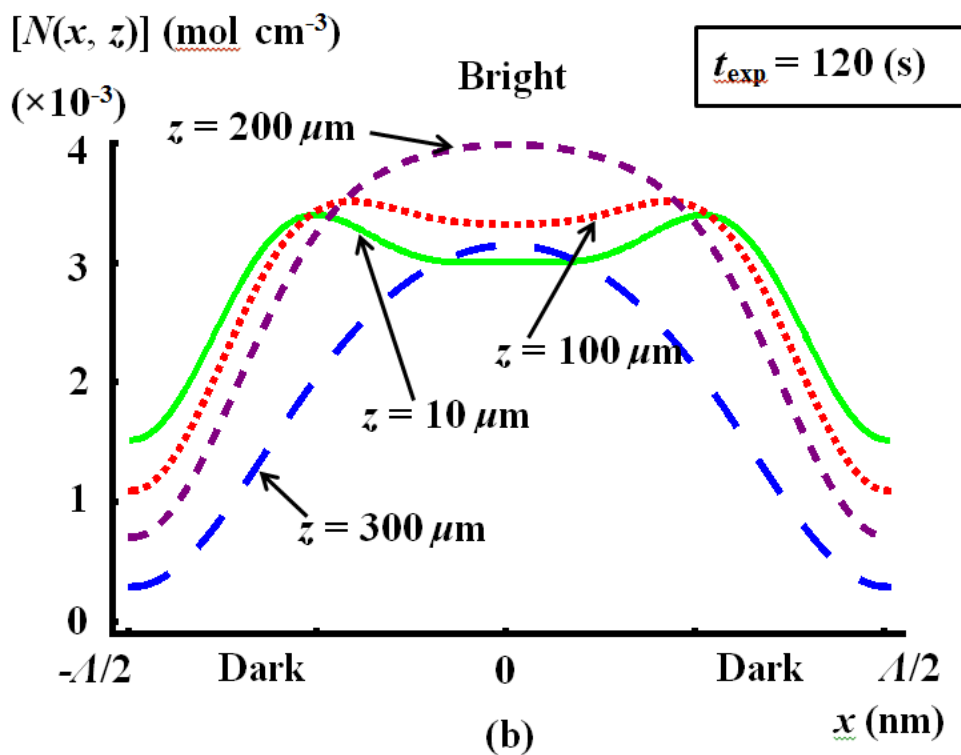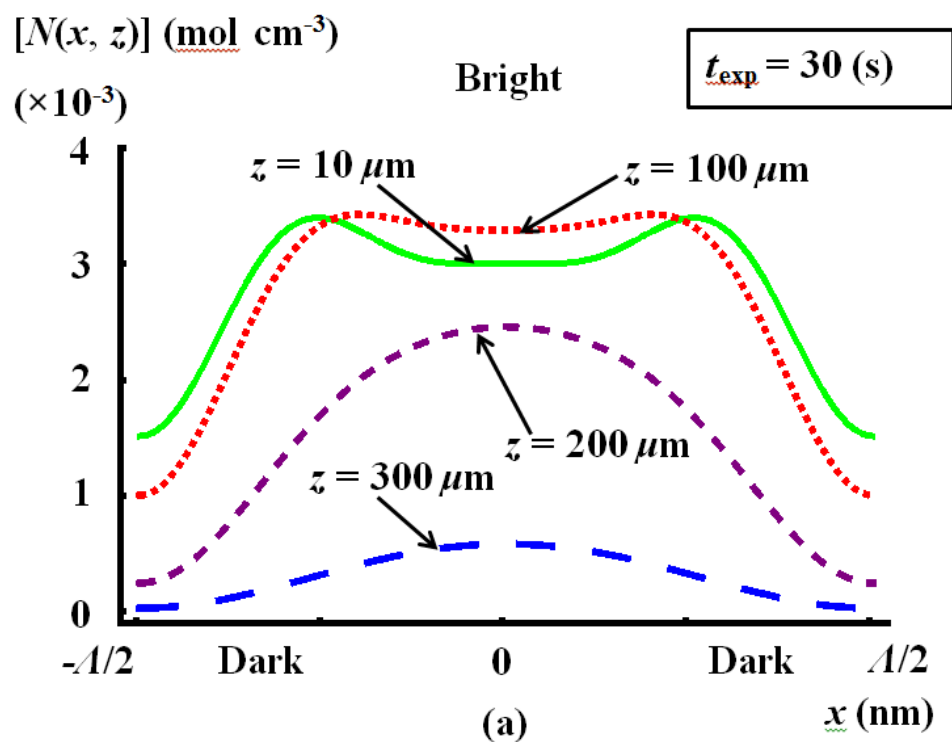
Figure 5. (color online) Evolution of formed photoproduct distributing in *x-z* axis [$N(x, z)$] mol cm$^{-3}$, for two different exposure times: case (a) $t_{exp}$ = 30 s and case (b) $t_{exp}$ = 120 s, for four different material depths: $z$ = 10 $\mu$m (green full curve); $z$ = 100 $\mu$m (red short dashed curve); $z$ = 200 $\mu$m (purple dashed curve); and $z$ = 300 $\mu$m (blue long dashed curve).

Using the same simulation parameter values and physical conditions into the extended 3-dimensiocal calculation model, the time varying evolution of produced photopolymer concentrations distributing in $x$-$z$ axis, $[N(x,z,t)]$, can be predicted and presented in Figure 5. In order to demonstrate the nonlinear response inside the material and the non-uniform characteristics of the photo-production in depth, comparisons are made for four different material depths in two different exposure time cases as observed in Figure 5.

In case (a) $t_{exp} = 30$ s, for short exposure time, as closing to the layer surface the exposure intensity is increasing, which not only causes a more rapid consumption of monomers, resulting in stronger concentration gradients, and giving rise to monomer diffusion[37] but also increases the dye consumption close to the dark region. Thus the corresponding nonlinear effects are also increasing as the photoreactions involving in less depth. When the material is closing to the surface, due to the increasingly nonlinear effects comparing to the thicker positions, the spatial distribution of the polymer concentration is not sinusoidal but significantly distorted from ideal sinusoidal behavior. As explained by Shui et al. [37], in bright region the rate of the monomers being polymerized is more significant comparing to the rate of monomers diffusing in from the dark region and the formatting polymer concentration spatial distributions have distortion due to the high intensity exposure. As can be observed from Figure 5 such distortion is visible more obvious for thinner depth. When the depth is $z = 10$ $\mu$m (green full curve), a sunk part appears in the center and peaks rise on the both sides of the spatial polymer concentration distributions. This is because, in this situation any monomers diffusing into bright region are rapidly polymerized by the abundant available primary radicals before they can diffuse further into the central area of the exposing patterns [37, 38]. When the depths are $z = 200$ $\mu$m (purple dashed curve) and 300 $\mu$m (blue long dashed curve), these concentration curves all obey sinusoidal distribution, and the concentration amplitudes are attenuating as the depth increasing. It indicates that for the thicker positions, above discussed nonlinear effects are not so significant and such distortions are visibly weaker. In case (b) $t_{exp} = 120$ s, as can be illustrated in Figure 5, in additional to the discussed distortions due to the nonlinear effects, it is noting that the peaks of polymer concentration amplitude for $z = 200$ $\mu$m is larger than others and a similar sunk part appears in $z = 100$ $\mu$m for long exposure time. For the depth in $z = 200$ $\mu$m, on the basis of this analysis there are not so many ground state dye molecules being excited due to the low intensity, hence fewer radicals are produced. When the monomers in the dark region are diffusing into the bright region, the polymerization rate, $R_p = [M^\bullet][u]$, is not rapid for the low produced macro-radicals concentration, because there are not enough available primary radicals being generating after a long time exposure. Therefore these diffusion monomers are not used up and they are able to diffuse further into the central area of the exposing patterns, and there will not appear the sunk part in the center and peaks rise on the both sides as $z = 10$ $\mu$m and 100 $\mu$m. As the exposure continuing, in depth of $z = 200$ $\mu$m, the ground sate dye molecules in the bright region are consumed continuously and mildly, producing a small quantity of radicals all the exposure time, and there are always remaining some dye molecules in the center of the bright region. As a result, the diffusing monomers from the dark region can always be provided to the polymerization in the center of the bright region, thus the peak of the produced polymer concentration amplitude is larger than thinker positions. However, when closing to the layer surface, more dye molecules are consumed, and for long exposure time the dye concentration is insufficient in the bright region, especially in the center of the bright region, which leads to fewer primary radicals can be generated in this area, and the polymerization rarely occurs under this situation.

Finally, the refractive index of the non-uniform volume grating formatted in the material depth can be calculated applying the Lorenz-Lorenz relationship [22, 24]. Using the model by numerically solving for time varying $[u(x,z,t)]$ and $[N(x,z,t)]$, and then substituting these spatial concentrations into Eq. (32), a 3-dimensioanl time varying refractive index $n(x,z,t)$ spatial distribution is presented in Figure 6, plotted across two grating periods $-\Lambda \leq x \leq \Lambda$ and the thickness $0 \leq z \leq 300$ $\mu$m, for four exposure times, (a) $t_{exp} = 10$ s; (b) $t_{exp} = 30$ s; (c) $t_{exp} = 60$ s; and (d) $t_{exp} = 120$ s. In order to more completely examine the non-uniform grating formation, the perturbation refractive index $\Delta n$, defining that $\Delta n = n_{max} - n_{min}$, is also represented in Figure 7, with the same initial conditions. In Figure 6 and 7, it is obviously that the refractive index profile is not a simple attenuation trend. On the basis of the analyses presented above, there will be a non-uniform and non-sinusoidal volume grating formatted in depth. This distortion is visibly stronger when closing the layer surface. From Figure 6, in the centre of the dark region, it can be observed that the amplitude of refractive index still increases especially for long exposure time. It is also notable that as the long exposures taking place, the refractive index variation $\Delta n$ along $z$-axis is not monotonously attenuating as the material more depth, as observed in Figure 7.
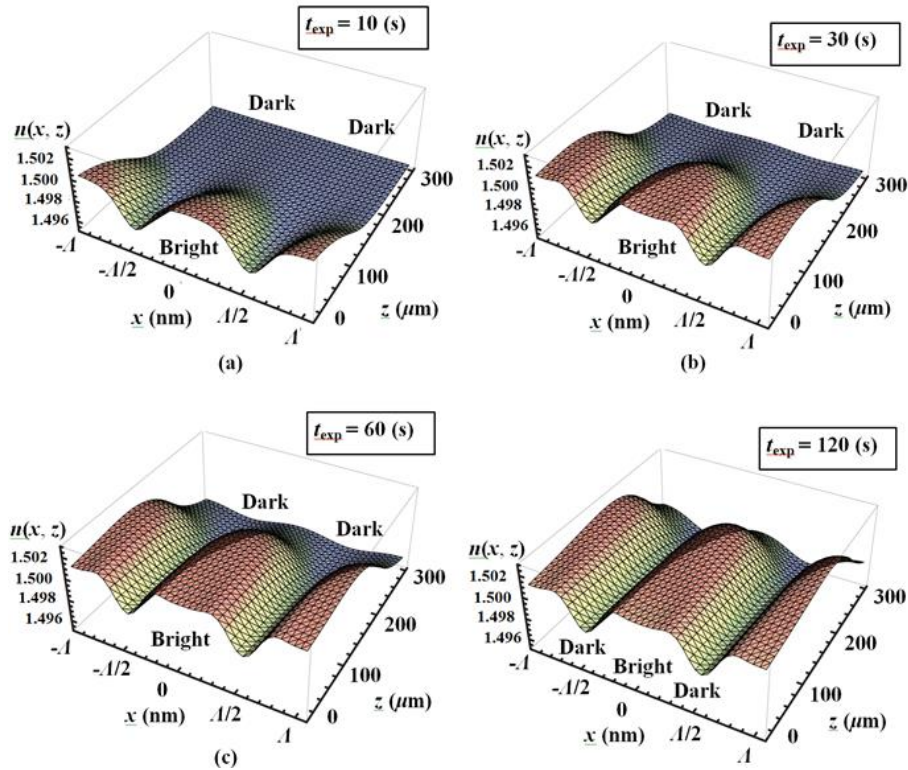
Figure 6. Simulation results of the refractive index $n(x, z, t)$ distribution in $x$-$z$ axis, for four different exposure times: case (a) $t_{exp} = 10$ s; case (b) $t_{exp} = 30$ s; case (c) $t_{exp} = 60$ s; and case (d) $t_{exp} = 120$ s.
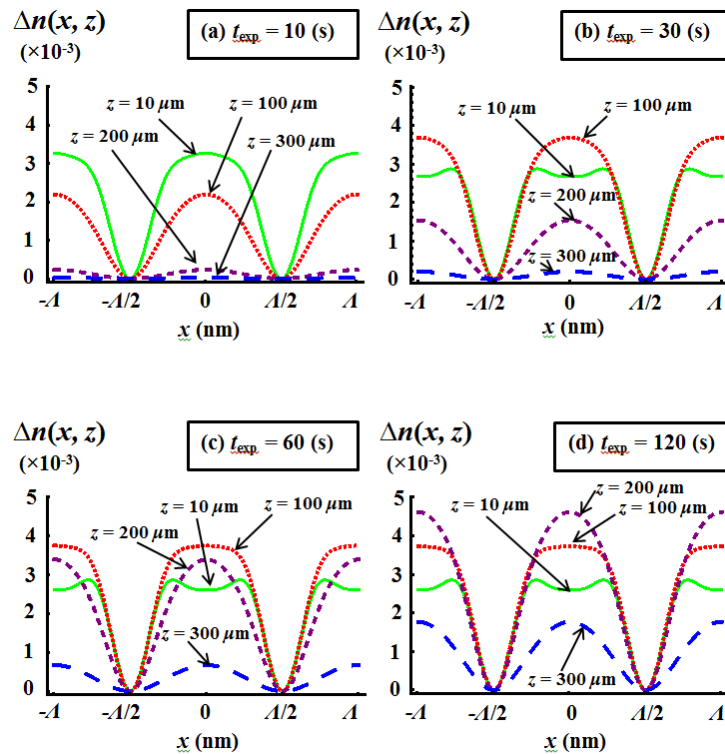


Figure 7. (color online) Simulation results of the refractive index modulation $\Delta n(x, z, t)$ distribution in $x$-$z$ axis, for four different exposure times: (a) $t_{exp} = 10$ s; (b) $t_{exp} = 30$ s; (c) $t_{exp} = 60$ s; and (d) $t_{exp} = 120$ s.

# 5. CONCLUSIONS

In this paper, some further developments of the 3-dimensional non-local photo-polymerization driven diffusion model are presented, and then the system partial differential rate equations, which govern the spatial and temporal concentration variations of each associated chemical species, are solved using the finite difference approximation. Following a detailed of analysis of major time varying photo-polymerization in material depth, the refractive index, indicating that there has the non-uniform deviations and non-linear distortions grating formatting in depth, is derived using the model. A comparison for different exposure times is also discussed and analysed in the cases of different material depth and a more complete and physical representation of material behaviour is obtained.

For standard AA/PVA photopolymer material this 3-dimensioal extended model is significantly presented the inclusions of the following: (1) The pervious mentioned attenuation in depth of the refractive index profile [14–16, 25, 26] just appears in the early exposure time; however, as the exposure time continuing, for the multiple and complete initiation, termination and inhibition effects in material, the refractive index profile is not monotonously attenuating in depth. (2) Due to above discussed non-linear response, the resulting spatial distribution of refractive index is not sinusoidal as exposing pattern but presenting the distortion form ideal sinusoidal behavior, and this distribution is visibly stronger when closing to the layer surface.

Further work remains to be done. A more complete and detailed quantum photo-physical and photochemical analysis of the photons absorption needs to be presented in the photo-initiation process. Comparisons the predictions of this model to reproducible experimental data for more types of photopolymer materials are also necessary. The shrinkage and swelling effects involving volume variations in the material should be investigated. Furthermore, due to the non-sinusoidal grating formatted, the diffraction efficiency for such non-uniform and distorted grating is required to be studied more deeply, and the nonlocal response for the large thickness evolutions should be derived and examined mathematically.

# ACKNOWLEDGMENTS

# REFERENCES

[1] M. Kawabata, A. Sato, I. Sumiyoshi, and T. Kubota, "Photopolymer system and its application to a color hologram," Appl. Opt. **33**(11), 2152–2156 (1994).

[2] G. Zhao and P. Mouroulis, "Second order grating formation in dry holographic photopolymers," Opt. Comm. **115**, 528–532 (1995).

[3] D. J. Lougnot, and L. Lavielle, "Polymers for holographic recording. VI. Some basic ideas for modelling the kinetics of the recording process," Appl. Opt. **6**, 225–245 (1997).

[4] S. Blaya, L. Carretero, R. Mallavia, A. Fimia, and R. F. Madrigal, "Holography as a technique for the study of photopolymerization kinetics in dry polymeric films with a nonlinear response," Appl. Opt. **38**(6), 955–962 (1999).

[5] S. H. Lin, P. L. Chen, C. Chuang, Y. F. Chao, and K. Y. Hsu, "Volume polarization holographic recording in thick phenanthrenequinone-doped poly(methyl methacrylate) photopolymer," Opt. Lett. **36**, 3039–3041 (2011).

[6] M. Ortuño, S. Gallego, C. Garcı́a, C. Neipp, and I. Pascual, "Holographic characteristics of a 1-mm-thick photopolymer to be used in holographic memories," Appl. Opt. **43**(35), 7008–7012 (2003).

[7] S. Gallego, M. Ortuño, C. Garcı́a, C. Neipp, A. Márquez, A. Beléndez, and I. Pascual, "Characterization of polyvinyl alcohol_acrylamide holographic memories with a first-harmonic diffusion model," Appl. Opt. **44**(29), 6025–6010 (2005).

[8] H. Wang, J. Wang, H. Liu, D. Yu, X. Sun, and J. Zhang, "Study of effective optical thickness in photopolymer for application", Opt. Lett. **37**, 2241–2243 (2012).

[9] M. D. Goodner, H. R. Lee, C. N. Bowman, "Method for determining the kinetic parameters in diffusion-controlled free-radical homopolymerizations," Ind. Eng. Chem. Res. **36**(4), 1247–1252 (1997).

[10] M. D. Goodner and C. N. Bowman, "Modeling primary radical termination and its effects on autoacceleration in photopolymerization kinetics," Macromolecules **32**(20), 6552–6559 (1999).

[11] M. D. Goodner and C. N. Bowman, "Development of a comprehensive free radical photopolymerization model incorporating heat and mass transfer effects in thick films," Chem. Eng. Sci. **57**, 887–890 (2002).

[12] M. Ortuño, C. Neipp, S. Gallego, and A. Beléndez, "Linear response deviations during recording of diffraction grating in pohotpolymers," Opt. Exp. **17**(15), 13193–13201 (2009).

[13] S. Blaya, P. Acebal, L. Carretero, A. Murciano, and R. F. Madrigal, "An explanation for the non-uniform grating effects during recording of diffraction gratings in photopolymers," Opt. Exp. **18**(2), 799–808 (2010).

[14] S. Gallego, M. Ortuño, C. Neipp, A. Márquez, A. Beléndez, I. Pascual, J. V. Kelly and J. T. Sheridan, "Physical and effective optical thickness of holographic diffraction gratings recorded in photopolymers," Opt. Exp. **13**(6), 1939–1947 (2005).

[15] S. Gallego, M. Ortuño, C. Neipp, A. Márquez, A. Beléndez, I. Pascual, J. V. Kelly and J. T. Sheridan, "3 Dimensional analysis of holographic photopolymers based memories," Opt. Exp. **13**(9), 3543–3557 (2005).

[16] S. Gallego, M. Ortuño, C. Neipp, A. Márquez, A. Beléndez, E. Fernandez, and I. Pascual, "3-dimensional characterization of thick grating formation in PVA/AA based photopolymer," Opt. Exp. **14**(12), 5121–5128 (2006).

[17] M. R. Gleeson and J. T. Sheridan, "Nonlocal photopolymerization kinetics including multiple termination mechanisms and dark reactions. Part I. Modeling," J. Opt. Soc. Am. **B 26**(9), 1736–1745 (2009).

[18] M. R. Gleeson, S. Liu, R. R. Mcleod, and J. T. Sheridan, "Nonlocal photopolymerization kinetics including multiple termination mechanisms and dark reactions. Part II. Experimental validation reactions," J. Opt. Soc. Am. **B 26**(9), 1746–1754 (2009).

[19] M. R. Gleeson, S. Liu, J. Guo, and J. T. Sheridan, "Non-local photo-polymerization kinetics including multiple termination mechanisms and dark reactions: Part III. Primary radical generation and inhibition," J. Opt. Soc. Am. **B 27**(9), 1804–1812 (2010).

[20] J. Guo, M. R. Gleeson, S. Liu, and J. T. Sheridan, "Non-local spatial frequency response of photopolymer materials containing chain transfer agents: I. Theoretical modeling," J. Opt. **13**(9), 095601 (2011).

[21] J. Guo, M. R. Gleeson, S. Liu, and J. T. Sheridan, "Non-local spatial frequency response of photopolymer materials containing chain transfer agents: II. Experimental results," J. Opt. **13**(9), 095601 (2011).

[22] I. Aubrecht, M. Miler, and I. Koudela, "Recording of holographic diffraction gratings in photopolymers: Theoretical modelling and real-time monitoring of grating growth," J. Mod. Opt. **45**(7), 1467–1477 (1998).

[23] C. H. Depuy, O. L. Chapman, *Molecular reactions and photochemistry*, Prentice Hall, Inc., London, UK, 1–6 (1972).

[24] M. Born and E. Wolf, *Principles of Optics*, 7th ed. Cambridge University Press., London, UK, 75–115 (1999).

[25] C. Neipp, J.T. Sheridan, S. Gallego, M. Ortu~no, A. M_arquez, I. Pascual, and A. Bel_endez, "Effect of a depth attenuated refractive index profile in the angular responses of the efficiency of higher orders in volume gratings recorded in a PVA/acrylamide photopolymer," Opt. Comm. **233**, 311–322 (2004).

[26] F. T. O'Neill, J. R. Lawrence, and J. T. Sheridan, "Thickness variation of a self-processing acrylamide-based photopolymer and reflection holography," Opt. Eng. **40**, (2001).

[27] M. R. Gleeson, J. V. Kelly, C. E. Close, F. T. O'Neill, and J. T. Sheridan, "Effects of absorption and inhibition during grating formation in photopolymer materials," J. Opt. Soc. Am. **B 23**(10), 2079–2088 (2006).

[28] M. R. Gleeson, S. Liu, S. O'Duill, and J. T. Sheridan, "Examination of the photoinitiation processes in photopolymer materials," J. Appl. Phys. **104**(6), 104–111 (2008).

[29] S. Liu, M. R. Gleeson, and J. T. Sheridan, "Analysis of the photoabsorptive behavior of two different photosensitizers in a photopolymer material," J. Opt. Soc. Am. **B 26**(3), 528–536 (2009).

[30] Y. Qi, M. R. Gleeson, J. Guo, S. Gallego, and J. T. Sheridan, "Quantitative comparison of five different photosensitizers for use in a photopolymer," Phys. Res. Int. **2012**, 1–11 (2012).

[31] O. Kashin, E. Tolstik, V. Matusevich, and R. Kowarschik, "Numerical investigation of the (1 + 1)D self-trapping of laser beams in photometric films based on polymethylmethacrylate and phenanthrenequinone," J. Opt. Soc. Am. **B 26**(11), 2152–2156 (2009).

[32] J. Sheridan and J. Lawrence, "Nonlocal-response diffusion model of holographic recording in photopolymer," J. Opt. Soc. Am. **A 17**(6), 1108–1114 (2000).

[33] J. Kelly, M. Gleeson, C. Close, F. O'Neill, J. Sheridan, S. Gallego, and C. Neipp, "Temporal analysis of grating formation in photopolymer using the nonlocal polymerization-driven diffusion model," Opt. Exp. **13**(18), 6990–7004 (2005).

[34] S. Liu, M. R. Gleeson, D. Sabol, and J. T. Sheridan, "Extended model of the photoinitiation mechanisms in photopolymer materials," J. Appl. Phys. **106**, 104911, (2009).

[35] H. Kogelnik, "Coupled wave theory for thick hologram gratings," Bell Syst. Tech. J. **48**, 2909–2647 (1969).

[36] R. Kowarschik, "Diffraction efficiency of attenuated sinusoidally modulated grating in volume holograms," J. Mod. Opt. **23**(12), 1039–1051 (1976).

[37] S. Liu, M. R. Gleeson, J. Guo, and J. T. Sheridan, "High Intensity Response of Photopolymer Materials for Holographic Grating Formation," Macromolecules **43**(22), 9462–9472 (2010).

[38] S. Liu, M. R. Gleeson, J. Guo, J. T. Sheridan, E. Tolstik, V. Matusevich, and R. Kowarschik, "Modeling the photochemical kinetics induced by holographic exposures in PQ/PMMA photopolymer material," J. Opt. Soc. Am. B **28**(11), 2833–2843 (2011).